

PHYSICAL REVIEW D

PARTICLES AND FIELDS

THIRD SERIES, VOLUME 41, NUMBER 9

1 MAY 1990

ν_μ - ν_e universality in charged-current neutrino interactions

N. J. Baker,* S. A. Kahn, M. J. Murtagh, N. P. Samios, and M. Tanaka
Brookhaven National Laboratory, Upton, New York 11973

C. Baltay,† E. R. Hyatt, S. Manly,† and R. Steiner‡
Columbia University, New York, New York 10027

P. F. Jacques, M. Kalelkar, R. J. Plano, and P. E. Stamer§
Rutgers University, New Brunswick, New Jersey 08903

(Received 24 April 1989; revised manuscript received 21 December 1989)

A total of 1403 ν_e and 179 $\bar{\nu}_e$ charged-current interactions with energies ranging up to 200 GeV were observed in a wideband neutrino-beam experiment using the Fermilab 15-ft bubble chamber filled with a heavy Ne-H₂ mix. As a test of ν_μ - ν_e universality, these events were compared to samples of ν_μ and $\bar{\nu}_\mu$ charged-current events obtained during the same experiment. The ν_e -to- ν_μ cross-section ratio was measured to be 1.09 ± 0.17 , and the corresponding ratio for antineutrinos was 1.46 ± 0.34 . Kinematic distributions and charged-particle multiplicities were also consistent with universality. The neutral-strange-particle production rate was measured to be $(11.7 \pm 1.2)\%$ for ν_e and $(5.2 \pm 2.2)\%$ for $\bar{\nu}_e$, in good agreement with the ν_μ and $\bar{\nu}_\mu$ rates. The relative rate for e^-e^+ dilepton production by ν_e was $(0.82 \pm 0.47)\%$, also consistent with universality. The rate for neutral-strange-particle production in e^-e^+ dilepton events is reported for the first time. The measured rate of 0.64 ± 0.45 agrees with the value expected from universality.

I. INTRODUCTION

The results of a study of ν_μ - ν_e universality in charged-current neutrino interactions in the 15-ft bubble chamber at Fermilab are presented.¹ A total of 1403 ν_e and 179 $\bar{\nu}_e$ charged-current interactions were used for this study. This is an order-of-magnitude increase in statistics over any previously published similar work.

Universality is the hypothesis that the fermionic structures of the electromagnetic and weak interactions are the same for each generation. To an experimentalist it means that any observable differences between the e , μ , or τ , or the ν_e , ν_μ , or ν_τ , etc., are due solely to differences in mass. Theoretically, it allows the extension of the standard model of the electroweak interaction from one generation to many generations with relative ease.

The concept of leptonic universality has a strong experimental foundation. Contributions to this foundation come from many different sources, including measurements of the magnetic moment of the muon,² spectroscopy of bound muonic systems,³ comparisons of μ - p and e - p scattering results,⁴ $e^+e^- \rightarrow l^+l^-$ cross-section measure-

ments,⁵ determinations of the ratio of $\Gamma(\pi \rightarrow e\nu_e)$ to $\Gamma(\pi \rightarrow \mu\nu_\mu)$,⁶ cross-section measurements of $W \rightarrow l\nu_l$ and $Z \rightarrow l^+l^-$ decays,⁷ measurements of the τ lifetime,⁸ electroweak interference experiments,⁹ and counter and bubble-chamber experiments using high-energy neutrino beams.¹⁰ These experiments vary widely in precision and energy. Those with the highest precision involve charged leptons, while neutrino universality is less clearly established. Muon-neutrino interactions are well understood. However, studies of electron-neutrino interactions have been hampered by low statistics as well as systematic problems such as electron identification and knowledge of the neutrino flux.

There are a number of theoretical models which predict violations of universality. Some examples are supersymmetry,¹¹ neutrino oscillations,¹² theories with heavy leptons¹³ or heavy, neutral generation-changing gauge bosons,¹⁴ mirror-fermion models,¹⁵ and theories which view the observed fermion universality as accidental.¹⁶ Some of these lead to a violation of neutrino universality without a violation of charged-lepton universality. The experimental detection of a breakdown in neutrino

universality might indicate the existence of one of these phenomena, necessitating an extension or a modification of the standard model. Alternatively, confirmations of universality provide constraints on various theories.

In Sec. II of this paper, some experimental details are presented. In Sec. III the basic event selection and background analysis are discussed. Section IV gives the results of the universality analysis. This section is broken into five subsections, one for each test of neutrino universality. Section IV A contains results of the ν_e and $\bar{\nu}_e$ charged-current cross-section measurements. In Sec. IV B kinematic distributions of the ν_e and $\bar{\nu}_e$ charged-current events are compared to those expected assuming universality. Section IV C gives the results of an analysis of neutral-strange-particle production in ν_e and $\bar{\nu}_e$ charged-current interactions. The charged-particle multiplicities of ν_e and $\bar{\nu}_e$ charged-current events are compared to those for ν_μ and $\bar{\nu}_\mu$ charged-current events in Sec. IV D. In Sec. IV E the results of a search for ν_e -induced e^-e^+ dileptons are described and a rate for this process is presented. In addition, the first measurement of a rate for neutral-strange-particle production in e^-e^+ dilepton events is reported. Finally, in Sec. V all the results are summarized and the conclusions of the analysis are presented.

II. EXPERIMENTAL PROCEDURE

The data used in this analysis come from experiment E53 at Fermilab. In this experiment, the 15-ft bubble chamber was exposed to a horn-focused wideband neutrino beam. There were two separate runs, referred to in this paper as E53A and E53B, respectively. The full E53 data sample was used for this work.

The neutrino beam was generated by 400-GeV protons incident on a target of Al_2O_3 for E53A and BeO for E53B. Positively charged secondary particles from the production target were focused by two magnetic horns in E53A and by a single horn for E53B. After focusing, the secondaries were allowed to decay in a 400-m decay space. The bubble chamber was separated from this decay space by one kilometer of Earth, which served to absorb all particles except the beam neutrinos. The resulting neutrino spectrum peaked at 20 GeV for ν_μ (20–40 GeV for ν_e) and extended out to approximately 200 GeV.

The bubble chamber was filled with a heavy Ne- H_2 mixture (64 at. % neon). The 40-cm radiation length in this mixture allowed for easy identification of electrons through bremsstrahlung and their characteristic spiral. The interaction length in this liquid is 125 cm, short enough to provide good muon-hadron separation.

The bubble chamber was roughly spherical with a diameter of 3.7 m and a total target mass of 25 tons. A 30-kG magnetic field uniform to 15% was present throughout the chamber volume. Events were photographed with three different cameras. A total of approximately 400 000 photographs were taken in the two runs. The estimated number of ν_μ charged-current events in the film is 200 000, split equally between E53A and E53B.

III. DATA SELECTION AND BACKGROUNDS

In an attempt to identify ν_e and $\bar{\nu}_e$ charged-current interaction candidates, the film was scanned for all events with an e^- or e^+ coming from the vertex with a momentum greater than 300 MeV/c. To be identified as an e^- or e^+ , the track was required to exhibit at least two signatures characteristic of electrons in a heavy liquid. These signatures are bremsstrahlung with a $\gamma \rightarrow e^+e^-$ conversion, spiralization, production of a δ ray with energy comparable to the primary track, and e^+ annihilation with two $\gamma \rightarrow e^+e^-$ conversions. The selected events were measured and processed through the geometrical-reconstruction program TVGP (Ref. 17). In addition, the measured neutral-strange-particle decays (V^0 's) and γ conversions were passed through the kinematic-fitting program SQUAW. For each measured V^0 , SQUAW attempted to make constrained fits to the vertex for the following hypotheses: $K_S^0 \rightarrow \pi^+\pi^-$, $\Lambda^0 \rightarrow p\pi^-$, $\bar{\Lambda}^0 \rightarrow \pi^+\bar{p}$, and $\gamma p \rightarrow pe^+e^-$. For each measured γ only fits to the last hypothesis were attempted. Only those fits with a χ^2 per degree of freedom less than five were considered during later stages of the analysis.

After being scanned, measured, and reconstructed, each event containing an e^- or e^+ track was carefully edited by a physicist. At this stage the event reconstruction was checked and obvious background events were removed. In addition, fiducial volume cuts were made to remove events more than 125 cm above or below the mid-plane of the bubble chamber, events within 70 cm of the back wall of the chamber, and events within 10 cm of the wall of the bubble chamber. The first cut removed events close to the cameras and those near the bottom of the chamber. The large bubble size on the film for events close to the cameras and the loss of resolution for interactions far from the cameras prohibited accurate measurements for these events. The second cut was made to exclude events near the back wall of the chamber. This was necessary to ensure good particle identification, allow room for neutral particles to decay or interact, reduce the momentum measurement error on each charged track, and reduce the pion punchthrough background. The final cut decreased the possibility that the incoming neutral particle inducing the event was from an interaction in the bubble-chamber wall. The fiducial volume had a mass of 17 tons. The fiducial-volume cuts removed approximately one-quarter of the events, leaving 1754 events with an e^- and 685 events with an e^+ .

In the search for ν_e and $\bar{\nu}_e$ charged-current events, the backgrounds come from neutral-current (NC) and ν_μ - or $\bar{\nu}_\mu$ -induced charged-current events (ν_μ CC or $\bar{\nu}_\mu$ CC events) with an asymmetric Dalitz pair, or an asymmetric γ conversion, Compton electron, δ ray, or K_{e3} decay close to the vertex. Other K , π , and μ decays leading to an e^+ or e^- in the final state have been calculated to be negligible compared to K_{e3} decay. An additional background in the e^+ sample comes from ν_μ -induced charm production and its subsequent semileptonic decay, so-called μ^-e^+ dilepton events.

All of these backgrounds were substantially reduced by

requiring the e^- or e^+ track to have a momentum of at least 2 GeV/c. This cut was effective because all of the backgrounds arise from particles produced in the hadronic sector of the interaction. The momentum distributions of such particles drop off rapidly with increasing momentum. This cut removed 330 e^- and 220 e^+ events. The loss of good events due to this cut was estimated by a Monte Carlo technique that assumed universality and smeared the electron momenta using EGS4 (Ref. 18). This technique will be discussed in more detail in Sec. IV B. The loss was calculated to be $(6\pm 1)\%$ in each of the two samples.

The requirements that the angle between each e^- track and any other charged particle be greater than 4° and that the e^- have greater than one-half of the maximum kinematically allowed energy for a δ ray were sufficient to remove the remaining background due to δ rays. This cut removed 21 events from the e^- sample. The fraction of good events lost with this cut was estimated to be $(0.6\pm 0.6)\%$ by observing the loss of e^+ events using similar criteria. The 1403 e^- events remaining after this cut were considered to be ν_e charged-current interactions (ν_e CC sample).

Most of the μ^-e^+ background in the e^+ sample was removed by requiring that no event contain a negative track that leaves the bubble chamber (an L^- track). This cut was effective because most of the time the μ^- in the μ^-e^+ events leaves the bubble chamber without interacting. There are a small number of events (1–2%) where the muon has such a low energy that it can be trapped in the bubble chamber. The background in the $\bar{\nu}_e$ CC sample arising from this source was estimated to be 12 ± 4 events. The L^- cut removed 286 e^+ events. The remaining 179 e^+ events were considered to be $\bar{\nu}_e$ charged-current interactions ($\bar{\nu}_e$ CC sample). There was a significant loss of legitimate $\bar{\nu}_e$ CC events from the L^- cut due to negative hadrons which left the chamber before interacting. This loss was calculated from the remaining $\bar{\nu}_e$ CC events. For each event in the $\bar{\nu}_e$ CC sample with N interacting negative (I^-) tracks, a weight was calculated. This weight represented the probability that any of the N I^- tracks leave the chamber mimicking a muon. Each weight was corrected for those $\bar{\nu}_e$ events already lost from the sample by dividing the weight by the probability that none of the I^- tracks leave the chamber. The sum of these weights for all the $\bar{\nu}_e$ events represented the number of $\bar{\nu}_e$ CC events lost due to the L^- cut. This calculation yielded a loss of $(20\pm 4)\%$.

After making the aforementioned cuts, the remaining background was estimated to be 16 ± 3 events in the ν_e sample and 13 ± 5 events in the $\bar{\nu}_e$ sample. After subtraction of this background, the numbers of ν_e and $\bar{\nu}_e$ CC events were corrected for losses and efficiencies. In addition to the corrections described above it was also necessary to correct for the losses due to confused events, scanning efficiency, and electron-identification efficiency. The confused event loss arose from events that were too messy or confused to measure. The confusion came from many sources such as high track density, poor film quality, boiling in the liquid, overlapping events, etc. For the ν_e and $\bar{\nu}_e$ CC samples it was estimated to be $(10\pm 5)\%$ by examining scan and edit notes. The scanning efficiency was determined to be $(80\pm 5)\%$ by rescanning portions of the film. The electron-identification efficiency is the probability that an e^+ or e^- track have two identifying signatures. This probability has been determined as a function of momentum by examining converted gammas in the bubble chamber. The electron-identification efficiency is $(98\pm 2)\%$ for tracks with a momentum greater than 2 GeV/c. Table I summarizes the corrections for losses and efficiencies for the ν_e CC and $\bar{\nu}_e$ CC samples. The corrected numbers of events (N_c) are given by

$$N_c = N_o \frac{C_1 C_2 C_3 C_4}{C_5 C_6},$$

where N_o is the observed number of events and the correction factors, C_i , were calculated separately for each run. Values of C_i averaged over the two runs are given in Table I. This yielded 2089 ± 137 ν_e CC and 313 ± 32 $\bar{\nu}_e$ CC interactions in the fiducial volume for both runs combined.

The normalization samples of ν_μ CC and $\bar{\nu}_\mu$ CC events came from a scan of approximately 1.3% of the pictures scattered throughout the film. During this scan, the scanners measured any event in the bubble chamber induced by a neutral particle traveling in the ν -beam direction.

ν_μ CC events were defined to be events inside the fiducial volume which had $E_\nu > 10$ GeV and at least one negative leaving (L^-) track, where E_ν is defined to be the total visible energy of the event corrected for missing neutral energy as described in Sec. IV A. In addition, the fractional energy transfer to the hadronic system,

$$y = \frac{E_\nu - E_\mu}{E_\nu},$$

TABLE I. Efficiencies and corrections for the ν_e and $\bar{\nu}_e$ CC events.

Correction	ν_e	$\bar{\nu}_e$
C_1 , δ ray	1.006 ± 0.006	None
C_2 , $P_e > 2 \frac{\text{GeV}}{c}$	1.06 ± 0.01	1.06 ± 0.01
C_3 , L^-	None	1.25 ± 0.05
C_4 , confused event	1.10 ± 0.05	1.10 ± 0.05
C_5 , scan efficiency (both runs averaged)	0.80 ± 0.05	0.80 ± 0.05
C_6 , e^- (e^+) identification efficiency	0.98 ± 0.02	0.98 ± 0.02

was required to be less than 0.85 where the muon was assumed to be the highest-momentum L^- track. The energy cut was necessary to eliminate the background from neutrons and neutral strange particles. The y cut reduced the NC and $\bar{\nu}_\mu$ CC contamination. Events with high y had a relatively low lepton momentum and there was a significant background from NC and $\bar{\nu}_\mu$ CC events with hadrons that left the chamber (the so-called hadron punchthrough background).

Similarly, the $\bar{\nu}_\mu$ CC sample was defined to be those events inside the fiducial volume with $E_\nu > 10$ GeV, a leaving positive (L^+) track passing a y cut, and no L^- track. The requirement of no L^- track eliminated the background from ν_μ CC events and many NC events with hadron punchthrough. The y cut was 0.85 for E53B and 0.5 for E53A. The low value for the y cut in E53A was necessary because of the relatively small signal to background.

Those events not satisfying the ν_μ CC or $\bar{\nu}_\mu$ CC event requirements were placed in the "neutral-current" (NC) sample. This is somewhat of a misnomer since no attempt was made to isolate true neutral-current events in this analysis.

Having defined the various categories in the manner described above, the normalization sample yielded 1501 ν_μ CC candidates, 99 $\bar{\nu}_\mu$ CC candidates, and 499 NC candidates. The ν_μ CC sample still contained a significant contamination of NC and $\bar{\nu}_\mu$ CC events with a negative leaving hadron. Likewise, the $\bar{\nu}_\mu$ CC sample had a significant background from NC events with a leaving positive hadron. These contaminations had to be taken into account when calculating the final numbers of events as well as in the creation of event distributions for each sample.

The punchthrough backgrounds and losses in the ν_μ CC and $\bar{\nu}_\mu$ CC samples were handled in a statistical manner. The data were used to construct weighted fictitious or "simulated" events which yielded estimates for the corrections and backgrounds in both the rates and distributions. For example, the NC punchthrough into the ν_μ CC sample was estimated by constructing a new sample of events from those events in the NC sample that had at least one interacting negative track that would have passed the y cut had it left the bubble chamber. Each of the events in this new sample was weighted by the probability that the negative track leave the chamber and corrected for those events missing from the NC sam-

ple because they were identified as ν_μ CC events. The distributions and rate of these newly created events were subtracted from those of the ν_μ CC sample as background.

More explicitly, the background in the ν_μ CC sample was estimated by making weighted distributions of simulated events. N simulated events were created for each NC or $\bar{\nu}_\mu$ CC event with $E_\nu > 10$ GeV and with N interacting negative (I^-) tracks that passed the $y < 0.85$ cut (calculated assuming each I^- track to be the lepton). Only $\bar{\nu}_\mu$ CC events with $y < 0.5$ were considered to lessen the effect of the considerable high- y NC punchthrough in the $\bar{\nu}_\mu$ CC sample in this calculation. Events with high y had a relatively low μ^+ momentum and there was a significant background from low-momentum π^+ tracks that left the chamber in the NC events. For E53A, where the defining y cut for the $\bar{\nu}_\mu$ sample was 0.5, this procedure was rigorously correct. For E53B, the defining y cut was 0.85 and the signal to background was larger. The contribution of the events with $0.5 < y < 0.85$ to the corrections involving the $\bar{\nu}_\mu$ sample was negligible. The i th simulated event was created assuming the i th I^- track to be the lepton. The i th event weight w_i was calculated as

$$P_i = e^{-d_i/125},$$

$$\bar{P}_i = \prod_{\substack{j=1 \\ j \neq i \\ E_j > E_i}}^N (1 - e^{-d_j/125}),$$

$$S_i = \prod_{j=1}^N (1 - e^{-d_j/125}),$$

and

$$w_i = \frac{P_i \bar{P}_i}{S_i},$$

where d_i is the extrapolated track length to the bubble-chamber wall in cm. The distributions and rate of these weighted, simulated events were subtracted from those of the initial ν_μ CC sample.

The punchthrough background for the $\bar{\nu}_\mu$ CC sample was calculated in a similar fashion. Here, N simulated events were created for each NC event with $E_\nu > 10$ GeV, no L^- tracks, and N I^+ tracks passing the y cut assuming each to be the lepton. W_i for the i th simulated event

TABLE II. Punchthrough corrections for the ν_μ and $\bar{\nu}_\mu$ CC samples.

Sample	Observed events	NC $\rightarrow \nu_\mu$	NC $\rightarrow \bar{\nu}_\mu$	$\bar{\nu}_\mu \rightarrow \nu_\mu$	$\bar{\nu}_\mu \rightarrow$ NC	Corrected events
E53A						
ν_μ ($y < 0.85$)	863	-28	0	-1	0	834
$\bar{\nu}_\mu$ ($y < 0.50$)	17	0	-4	0	+5	18
E53B						
ν_μ ($y < 0.85$)	638	-32	0	-1	0	605
$\bar{\nu}_\mu$ ($y < 0.85$)	82	0	-23	+1	+14	74

TABLE III. Efficiencies and corrections for the ν_μ CC and $\bar{\nu}_\mu$ CC events.

Correction	ν_μ	$\bar{\nu}_\mu$
E53A		
$C_1, E_\nu > 10$ GeV	1.07 ± 0.01	1.03 ± 0.005
$C_2, y < 0.85$ for ν_μ	1.13 ± 0.013	None
$C_2, y < 0.5$ for $\bar{\nu}_\mu$	None	1.24 ± 0.024
C_3 , confused event	1.05 ± 0.05	1.05 ± 0.05
C_4 , scan efficiency	0.90 ± 0.05	0.90 ± 0.05
E53B		
$C_1, E_\nu > 10$ GeV	1.06 ± 0.01	1.03 ± 0.005
$C_2, y < 0.85$	1.13 ± 0.013	1.05 ± 0.005
C_3 , confused event	1.05 ± 0.05	1.05 ± 0.05
C_4 , scan efficiency	0.90 ± 0.05	0.90 ± 0.05

(assuming the i th I^+ track to be the lepton) was calculated as above. The distributions and rate of these weighted, simulated events were subtracted from those of the initial $\bar{\nu}_\mu$ CC sample.

In addition, the $\bar{\nu}_\mu$ CC sample was corrected for losses due to punchthrough. The loss to the ν_μ CC sample was just the $\bar{\nu}_\mu$ punchthrough contamination of the ν_μ CC sample calculated above. The same weighted distributions were added to the original $\bar{\nu}_\mu$ distributions and the $\bar{\nu}_\mu$ rate was adjusted slightly to take into account this loss. The loss to the NC sample occurred when a negative hadron in a good $\bar{\nu}_\mu$ CC event left the chamber where the calculated y (assuming the L^- track to be the μ^-) was greater than 0.85. To calculate this loss, N weighted, simulated events were created for each $\bar{\nu}_\mu$ CC event with $y < 0.5$ (assuming the fastest L^+ track to be the μ^+) and with $N I^-$ tracks having $y > 0.85$ (where y is calculated taking each I^- track to be the μ^-). Weighted distributions of these events were added to the original $\bar{\nu}_\mu$ CC event distributions to correct for this loss. The $\bar{\nu}_\mu$ CC rate was adjusted as well. The punchthrough event rate corrections are summarized in Table II.

The normalization samples were corrected for the energy and y cuts as well as for the confused event loss and scanning efficiency. The losses due to the 10-GeV energy cut were estimated by using the beam Monte Carlo simulation described in Sec. IV A below. The losses due to the y cuts were determined from the Buras and Gaemers parametrization of $\sigma(x, y)$ for ν_μ and $\bar{\nu}_\mu$ charged-current interactions with radiative corrections (see Sec. IV B). The confused event loss was estimated to be $(5 \pm 5)\%$. This loss was larger in the ν_e and $\bar{\nu}_e$ CC samples because the presence of converted bremsstrahlung gammas from the $e^-(e^+)$ added to the confusion. The scanning efficiency for these events was determined by rescanning part of the film. The corrected numbers (N_c) were given by

$$N_c = N_o \frac{C_1 C_2 C_3}{C_4},$$

where N_o is the observed number of events and the C_i are as defined in Table III. After correcting for all efficiencies, cuts, and backgrounds there were 2021 ± 121 events in the ν_μ CC sample and 120 ± 19 events in the $\bar{\nu}_\mu$ CC sample. Scaling these normalization numbers up to

represent the total data sample, there were $147\,000 \pm 9\,100$ ν_μ and $9\,560 \pm 1\,430$ $\bar{\nu}_\mu$ charged-current interactions inside the fiducial volume in this experiment.

IV. RESULTS

A. Cross sections

In order to determine the cross sections for ν_e and $\bar{\nu}_e$ charged-current interactions, it was necessary to calculate the ν_e/ν_μ and $\bar{\nu}_e/\bar{\nu}_\mu$ flux ratios. This was done using a Monte Carlo simulation of the neutrino beam. The K/π production spectrum that was used in this program was from Malensek.¹⁹ It is an empirical formula for thick target particle production based on a fit utilizing the data of Atherton *et al.*²⁰ These data consist of measurements of secondaries from p -Be collisions at 400 GeV/c for target lengths of 10, 30, and 50 cm. For E53B, Malensek's parametrization was sufficient because the length and material of the target was the same as that used by Atherton *et al.* However, for E53A an Al_2O_3 target was used and Malensek's parametrization was adjusted slightly to take this difference into account. The correction was based on measurements by Eichten *et al.*²¹ of secondary particle production by protons incident on different materials. For a given secondary particle momentum and type, the Malensek production formula output was scaled by the measured secondary production for Al_2O_3 divided by that for Be as given by a linear fit to the data of Eichten *et al.* This correction ranged from 0.8 to 1.1.

Atherton *et al.* have estimated their errors for the K and π measurements to be approximately 8%. Malensek's formula typically agrees with the data from Atherton *et al.* to 5%. Eichten *et al.* estimate the errors in their reported production ratios to be 4%. Adding these errors in quadrature gives a conservative overall error in the particle production of 10%. This was the dominant error in the beam Monte Carlo calculations used in this analysis.

Figure 1 shows the ν_μ CC event energy spectrum shape predicted by the beam Monte Carlo simulation superimposed on the data for E53B. The plot for E53A is similar. The data have been corrected for missing neutral energy using a simple method determined in a narrow-band neutrino beam experiment by the same group in the same

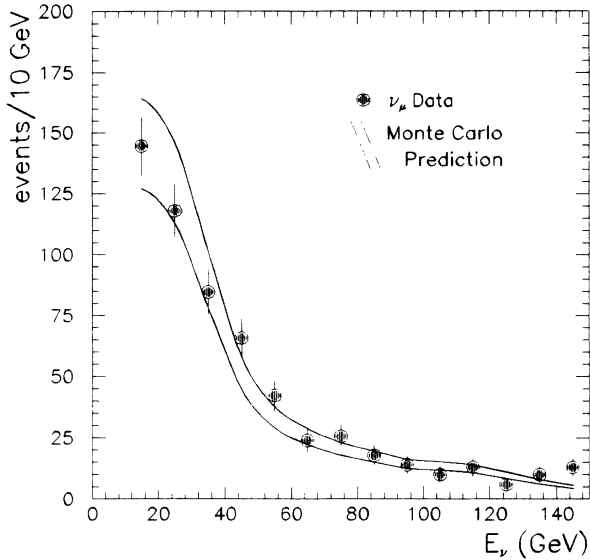


FIG. 1. E_ν spectrum for E53B ν_μ CC events. The points indicate the data and the outlined region is the one-standard-deviation boundary for the distribution predicted by the Monte Carlo simulation.

chamber with the same heavy Ne-H₂ fill.²² This correction is summarized as

$$E_h < 20 \text{ GeV}, \quad E_h^c = 1.11E_h ;$$

$$20 \text{ GeV} \leq E_h \leq 100 \text{ GeV}, \quad E_h^c = (0.003E_h + 1.05)E_h ;$$

$$E_h > 100 \text{ GeV}, \quad E_h^c = 1.35E_h ;$$

where E_h is the visible hadronic energy and E_h^c is the hadronic energy corrected for missing neutral energy. The average correction to the hadronic energy using this method is 14%. The errors in the data are statistical only. The one-standard-deviation boundaries for the beam Monte Carlo simulation reflect the production spectrum uncertainty as well as a 15% uncertainty in the hadronic energy of the data. These errors are conservative. The good agreement in Fig. 1 between the data points and the Monte Carlo calculation was a check on the beam Monte Carlo simulation.

Another check on the beam Monte Carlo simulation was the comparison between the predicted and observed $\bar{\nu}_\mu/\nu_\mu$ event ratios. For E53A, these numbers agreed within statistics. The observed ratio was $2.3 \pm 1.2\%$ and the predicted value was $0.83 \pm 0.08\%$. However, for E53B, reasonable agreement between these numbers was obtained only after decreasing the horn-focusing efficiency in the Monte Carlo program. Much effort was expended investigating this problem. The conclusion of this study was that something unexpected happened with the beam for E53B. Decreasing the focusing efficiency in the Monte Carlo program effectively corrected for some unknown problem with the beam, bringing the $\bar{\nu}_\mu$ CC rate into closer agreement with the data. When this was done, the ν_e CC and $\bar{\nu}_e$ CC rates also agreed with the data, consistent with universality. Because it is impossi-

ble to know exactly what was wrong with the beam, the data from E53B were not used for the ν_e and $\bar{\nu}_e$ charged-current cross-section measurements. It should be noted that the basic shapes of the Monte Carlo ν_e and $\bar{\nu}_e$ charged-current event energy spectra do not change significantly when the horn-focusing efficiency is reduced. Therefore the data from both runs were used for the kinematic distribution comparison. The other tests of universality presented in this paper are not dependent on the beam Monte Carlo simulation.

For E53A, the beam calculation gave the relative fluxes

$$\frac{\bar{\nu}_\mu}{\nu_\mu} = (1.24 \pm 0.12)\%, \quad \frac{\nu_e}{\nu_\mu} = (0.59 \pm 0.06)\%,$$

$$\frac{\bar{\nu}_e}{\nu_\mu} = (0.09 \pm 0.01)\% .$$

After energy weighting, these flux ratios, the world average ν_μ and $\bar{\nu}_\mu$ charged-current cross sections,²³ and the measured ν_e and $\bar{\nu}_e$ event rates were used to derive

$$\frac{\sigma(\nu_e)}{\sigma(\nu_\mu)} = \frac{(\nu_e \text{ events observed}) \int E_{\nu_\mu}(\nu_\mu \text{ flux})dE}{(\nu_\mu \text{ events observed}) \int E_{\nu_e}(\nu_e \text{ flux})dE} = 1.09 \pm 0.17 .$$

This number can be interpreted as the cross-section ratio if the assumption is made that the cross section is proportional to energy for both types of neutrinos. A similar calculation for the antineutrinos yielded

$$\frac{\sigma(\bar{\nu}_e)}{\sigma(\bar{\nu}_\mu)} = 1.46 \pm 0.34 .$$

Within errors both ratios are close to one, consistent with neutrino universality.

B. Kinematic distributions

Figure 2 shows the raw or uncorrected ν_e candidate-event spectrum. The expected curve (assuming universality) as calculated by the beam Monte Carlo program is superimposed on the data. Note that the spectrum for the data is considerably softer than expected. This is in part due to the fact that the data in this plot have not been corrected for missing neutral hadronic energy. It is also due to mismeasurements of the electron momenta. In this experiment, particle momenta were measured by curvature in the magnetic field of the bubble chamber. Bremsstrahlung was not a problem for most of the particles because the bremsstrahlung probability goes as $1/m^2$, where m is the mass of the particle.²⁴ However, for high-energy electrons in the heavy liquid used for this experiment, bremsstrahlung often caused abrupt changes in curvature leading to poor momentum measurements. These mismeasurements distorted the interesting kinematic distributions, making it difficult to test universality directly.

This problem was overcome by comparing the data to kinematic distributions of simulated events constructed assuming universality and having $e^-(e^+)$ momenta

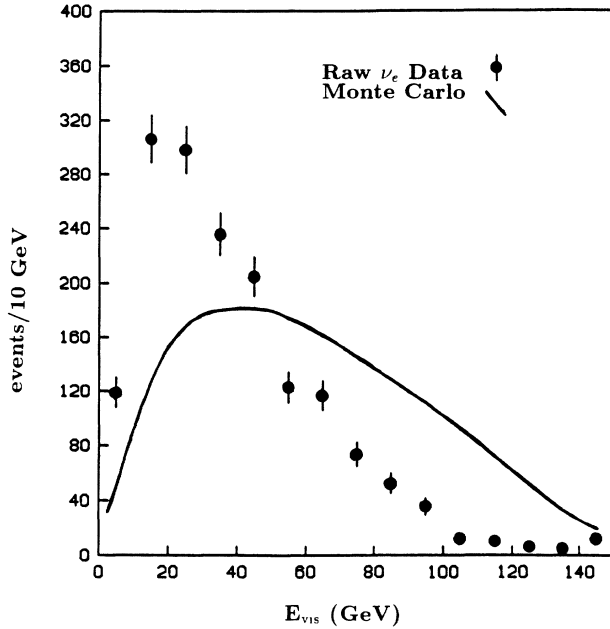


FIG. 2. Total visible energy E_{vis} for the raw ν_e candidate data. The points represent the data with statistical error only and the solid line represents the distribution expected from universality without electron momentum smearing.

smearing in an appropriate fashion. More explicitly, a large number of weighted Monte Carlo events were created to compare to the data. For each generated event, E_ν was picked flat between 0 and 200 GeV and weighted by the $\nu_e(\bar{\nu}_e)$ beam Monte Carlo spectrum described above. The kinematic variables

$$x = \frac{Q^2}{2M_p(E_\nu - E_e)}$$

and

$$y = \frac{E_\nu - E_e}{E_\nu}$$

were picked flat between 0 and 1. Each event was then weighted again by the production cross section $\sigma(x, y)/E_\nu$ for muon neutrinos (antineutrinos). Having chosen x , y , and E_ν , the magnitude and direction of the “true” e^- (e^+) momentum was completely specified for each event. This information was then input as the initial condition to the EGS4 Monte Carlo package which generated an e^- (e^+) shower starting at a random point within the bubble chamber. A total of 30 points along the primary track in this shower were chosen as “scanner measurement points.” The three-dimensional coordinates describing the position of each of these points in the bubble chamber were translated into three sets of two-dimensional coordinates, corresponding to the position of the point on the three film planes. This information was processed through the E53 version of TVGP, yielding a reconstructed or “measured” e^- (e^+) momentum for the given Monte Carlo event. This “measured” e^- (e^+) momentum was then used in place of the “true” e^- (e^+)

momentum as the weighted Monte Carlo distributions were created. These distributions were compared directly to the data as a test of universality.

The production cross section for $\nu_\mu(\bar{\nu}_\mu)$ charged-current interactions was obtained from the Buras and Gaemers parametrization with radiative corrections.²⁵ A conservative estimate of the error in this parametrization is 10%. This was obtained by comparing the parametrization to experimental data.²⁶

A check on the validity of this procedure was to use the same method to generate $\nu_\mu(\bar{\nu}_\mu)$ events and compare the Monte Carlo distributions to those obtained using the normalization data. Figures 1, 3(a), and 3(b) show such a comparison for muon neutrinos. The E_ν , x , and y distri-

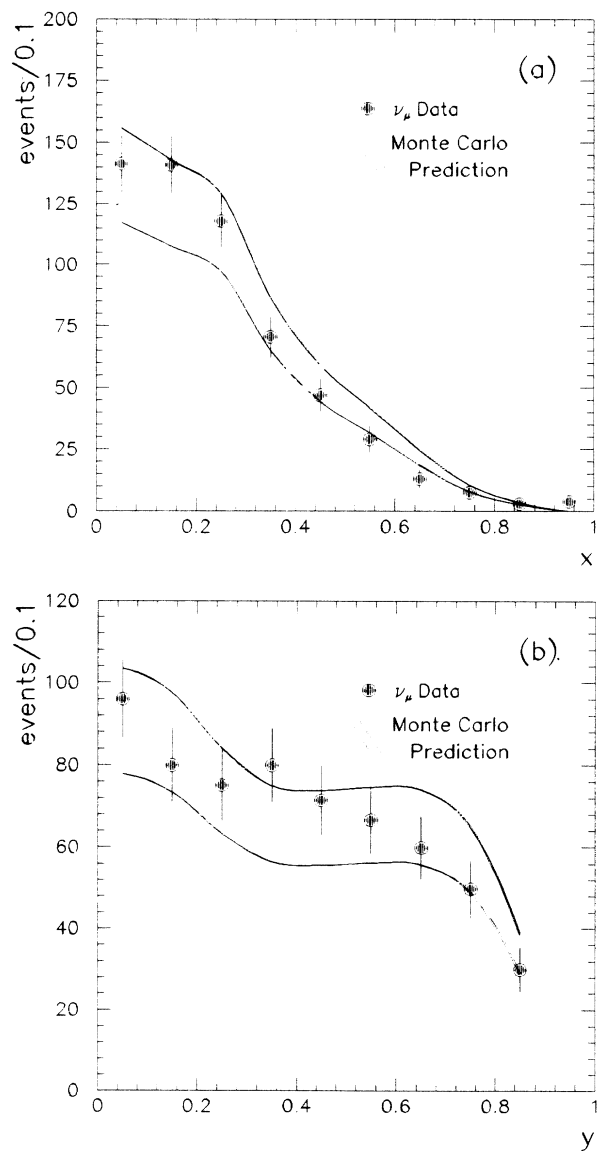


FIG. 3. Kinematic distributions for E53B ν_μ CC events. The points indicate the data and the outlined region is the one-standard-deviation boundary for the distributions predicted by the Monte Carlo simulation. (a) is the x distribution and (b) is the y distribution.

butions are given, respectively. The corresponding muon-antineutrino distributions are shown in Figures 4(a)–4(c). These plots are shown for E53B data because of the larger number of $\bar{\nu}_\mu$ events in that run. Except for the smaller number of $\bar{\nu}_\mu$ events, the plots for E53A are similar. The Monte Carlo distributions are area normalized to the data. As discussed earlier, the data distributions are background corrected. Also, the Monte Carlo distributions take into account cuts in the data. The hadronic energy in the data is corrected using the method described above. The errors in the data are statistical only. The errors in the Monte Carlo distributions reflect an 8% error in the beam Monte Carlo spectrum, a 10% error in the Buras and Gaemers parametrization, and a 15% uncertainty in the hadronic energy for the data.

The errors for the various distributions were determined by smearing the appropriate quantity and observing the change in the distributions. The one-standard-deviation error boundaries are shown for the Monte Carlo distributions. The only difference between the Monte Carlo method used for the $\nu_\mu(\bar{\nu}_\mu)$ events and that used for the $\nu_e(\bar{\nu}_e)$ events was that for the $\nu_\mu(\bar{\nu}_\mu)$ distributions the measured and true lepton momenta were assumed to be the same.

Kinematic distributions for the ν_e CC and $\bar{\nu}_e$ CC events are shown in Figs. 5 and 6. Monte Carlo distributions created using the method described above were superimposed on the data after being area normalized to the data. Only those gammas lying outside a 2.5° cone about the measured e^- (e^+) momentum are included in

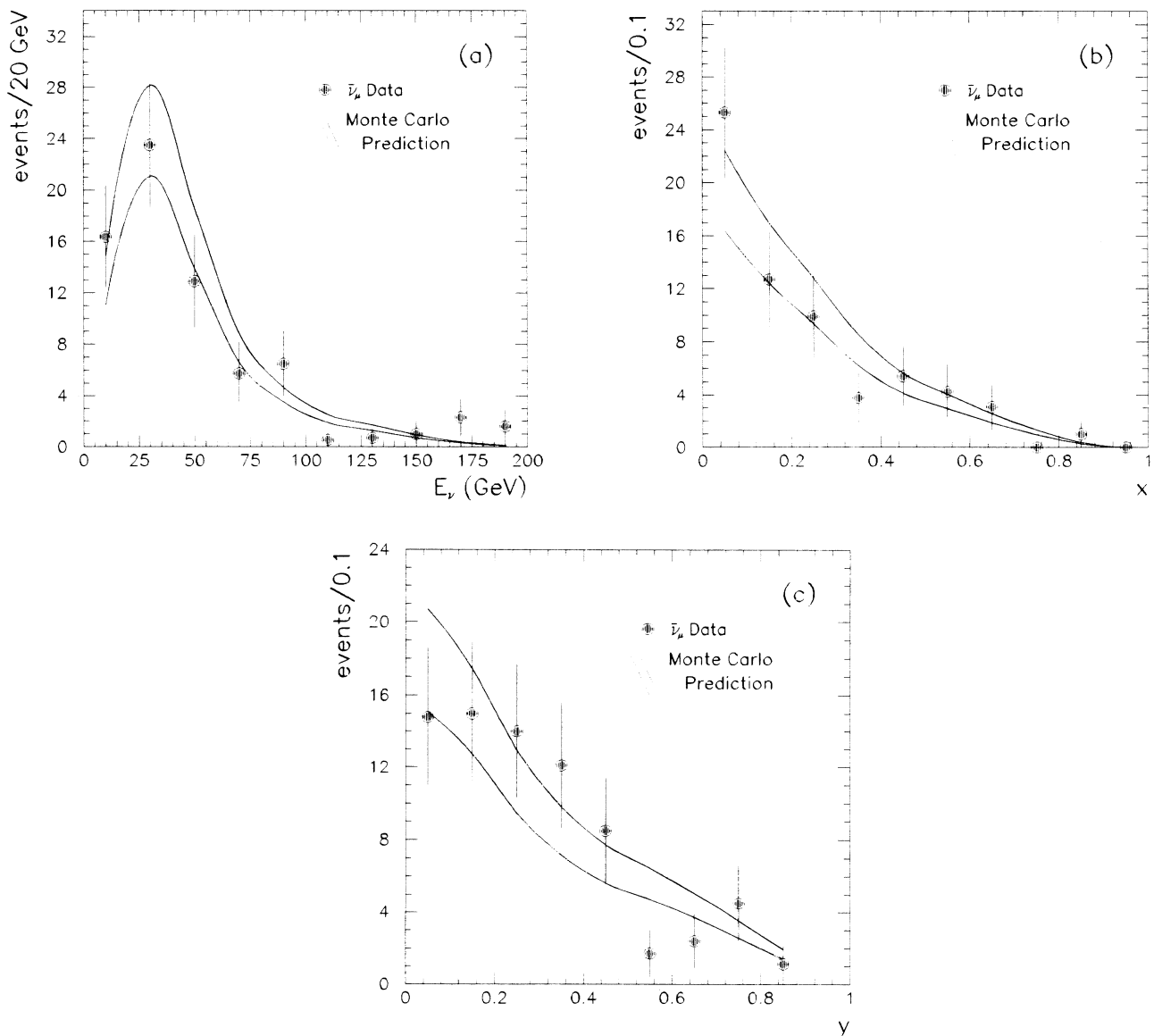


FIG. 4. Kinematic distributions for E53B $\bar{\nu}_\mu$ CC events. The points indicate the data and the outlined region is the one-standard-deviation boundary for the distributions predicted by the Monte Carlo simulation. (a) is the E_ν spectrum, (b) is the x distribution, and (c) is the y distribution.

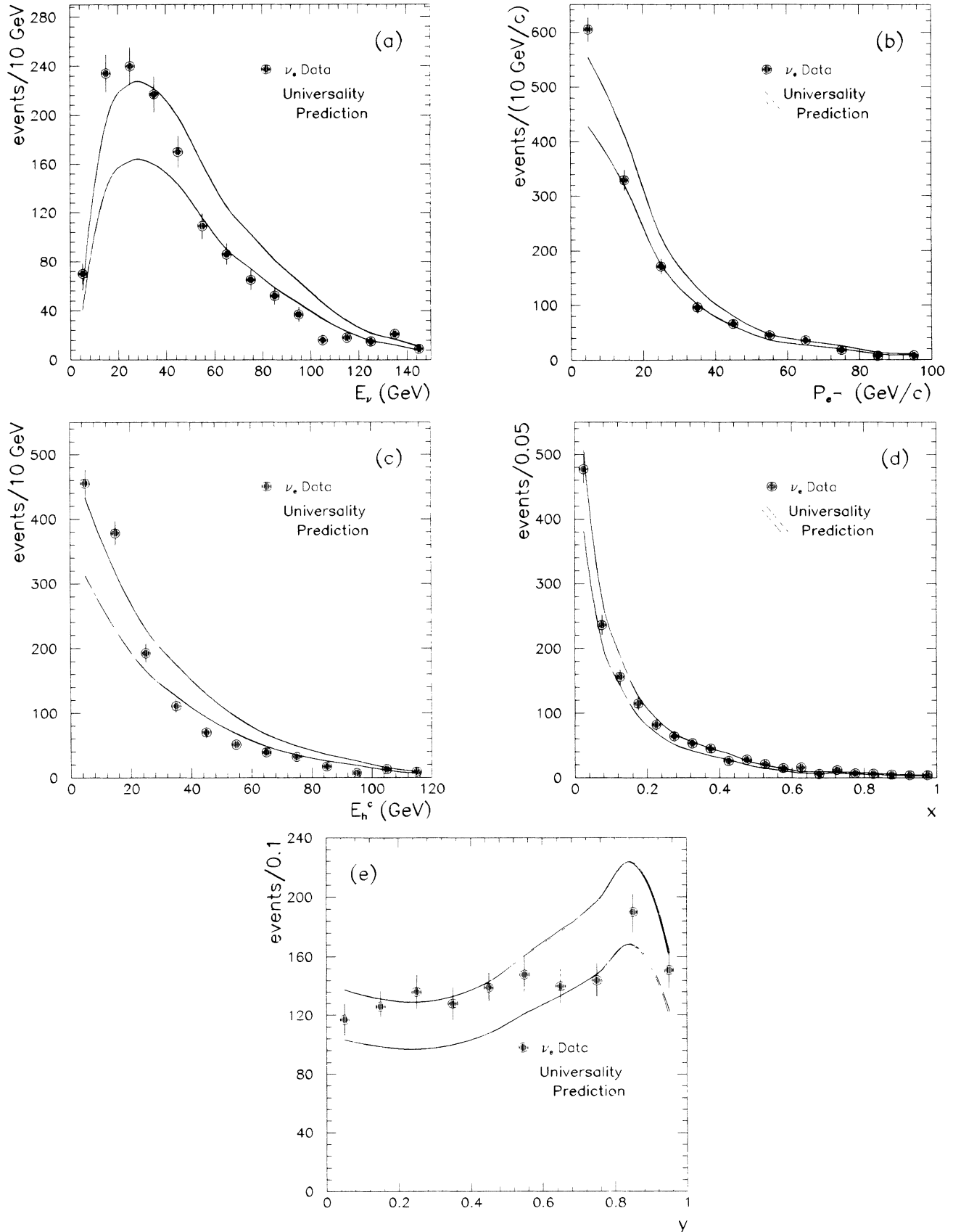


FIG. 5. Kinematic distributions for ν_e CC events. The points represent the data. The outlined region is the one-standard-deviation boundary for the distributions expected assuming universality. The plotted variables are (a) E_ν , (b) P_{e^-} , (c) E_h^e , (d) x , and (e) y .

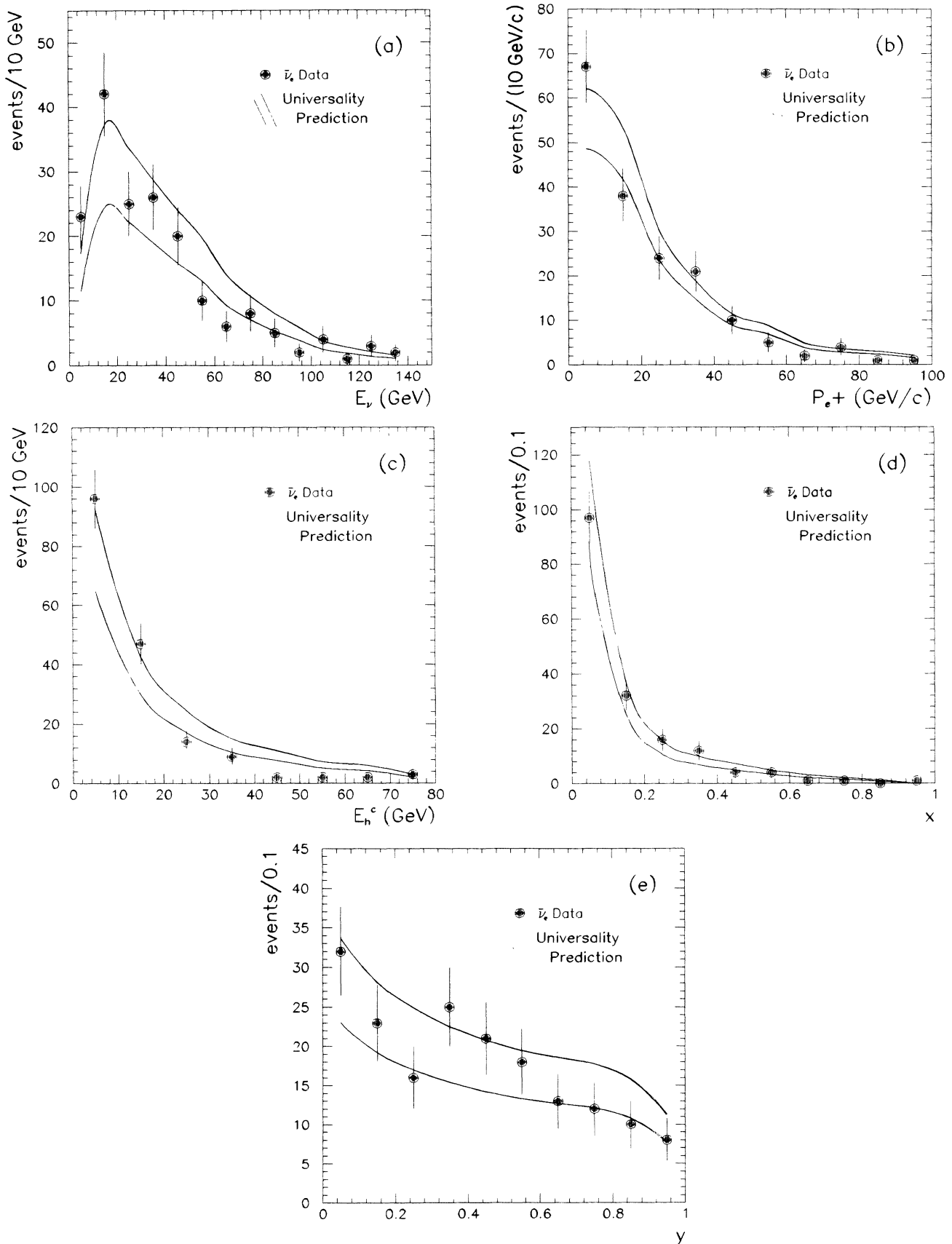


FIG. 6. Kinematic distributions for $\bar{\nu}_e$ CC events. The points represent the data. The outlined region is the one-standard-deviation boundary for the distributions expected assuming universality. The plotted variables are (a) E_ν , (b) P_{e^+} , (c) E_h^c , (d) x , and (e) y .

the hadronic energy. Those inside 2.5° were assumed to be converted bremsstrahlung gammas from the $e^-(e^+)$. In addition to the hadronic energy correction described in Sec. IV A, the hadronic energy in the ν_e CC data has been increased slightly to reflect the hadronic gamma and neutron-star measurement inefficiency in these events. An examination of the converted neutral energy per event as a function of the invariant mass of the charged hadrons showed that more neutral energy was measured in the ν_μ CC events than in the ν_e CC events. This discrepancy was interpreted as coming from a measurement inefficiency rather than a violation of universality. In general there is more activity on the film for the ν_e CC events due to converted bremsstrahlung gammas. This can lead to a converted hadronic gamma and neutron-star measurement inefficiency. So, the converted neutral energy per event as a linear function of the charged hadron invariant mass in the ν_e CC events was corrected to be the same as that for the ν_μ CC sample. This correction averaged 11% of the hadronic energy for the ν_e CC events. There were too few $\bar{\nu}_e$ CC events to use this method effectively; so the error in the hadronic energy was increased to 20% in the Monte Carlo $\bar{\nu}_e$ CC distributions.

The errors in the Monte Carlo distributions in Figs. 5 and 6 include an 8% error in the beam Monte Carlo spectrum, a 10% error in the Buras and Gaemers parametrization, and a total of 15% (20%) uncertainty in the hadronic energy of the $\nu_e(\bar{\nu}_e)$ CC data. The errors on the data points are statistical only and the one-standard-deviation error bands are shown for the Monte Carlo distributions. Within these errors, the data distributions agree very well with those expected assuming universality.

C. Strange-particle production

A search for neutral-strange-particle decays yielded 109 V^0 s in the 1403 ν_e CC events that remained after cuts. A similar search of the 179 $\bar{\nu}_e$ CC interactions revealed 7 V^0 s. Only those V^0 s with fits passing the χ^2 cut discussed in Sec. III were considered. In addition, the V^0 s were required to be farther than one cm from the neutrino vertex since the identification efficiency was poor in that region and to be farther than 10 cm from any wall to lessen the background from interactions in the walls of the bubble chamber. Finally, the calculated lifetime for each V^0 was required to be less than six proper lifetimes for that particular particle. To calculate the V^0 production rate it was necessary to correct the observed

number of V^0 s for losses and efficiencies. The appropriate corrections were determined in a previous E53 study of V^0 production by muon neutrinos.²⁷ They are summarized in Table IV. The corrected number of V^0 s (N_c) was given by

$$N_c = N_o \frac{C_1 C_2 C_3 C_4 C_5}{C_6 C_7},$$

where N_o is the observed number and the C_i are defined in Table IV. After the V^0 corrections, there were a total of 170 ± 18 V^0 s in 1403 ν_e CC events and 11.1 ± 4.1 V^0 s in 179 $\bar{\nu}_e$ CC events. Taking the weighted mean for both runs, these numbers yielded the following relative rates for neutral-strange-particle production:

$$\frac{\nu_e N \rightarrow e^- V^0 X}{\nu_e N \rightarrow e^- X} = (11.7 \pm 1.2)\%$$

$$\frac{\bar{\nu}_e N \rightarrow e^+ V^0 X}{\bar{\nu}_e N \rightarrow e^+ X} = (5.2 \pm 2.2)\%.$$

The comparable rates for ν_μ - and $\bar{\nu}_\mu$ -induced events are

$$\frac{\nu_\mu N \rightarrow \mu^- V^0 X}{\nu_\mu N \rightarrow \mu^- X} = (10.1 \pm 0.7)\%$$

$$\frac{\bar{\nu}_\mu N \rightarrow \mu^+ V^0 X}{\bar{\nu}_\mu N \rightarrow \mu^+ X} = (9.6 \pm 0.4)\%.$$

These rates were obtained by removing the branching ratio corrections from the strange-particle rates reported in Refs. 27 and 28. The $\nu_\mu V^0$ rate was adjusted from $(9.8 \pm 0.7)\%$ to take into account the harder ν_e flux. This adjustment consisted of folding in the known $\nu_\mu V^0$ rate as a function of energy with the ν_e -event energy spectrum predicted by the beam Monte Carlo simulation. A similar correction was not done for the $\bar{\nu}_\mu V^0$ rate because of the weak-energy dependence of the $\bar{\nu}_\mu V^0$ rate.²⁹ Within errors, the ν_e and $\bar{\nu}_e$ V^0 rates are consistent with neutrino universality.

D. Multiplicities

The average charged-particle multiplicity as a function of the square of the invariant mass of the charged particles (W_{ch}^2) is shown in Fig. 7 for the ν_e and ν_μ samples. The corresponding plot for the antineutrinos is shown in Fig. 8. The multiplicities are shown as functions of W_{ch}^2 because this quantity is independent of any lepton

TABLE IV. Correction factors for observed V^0 production.

Corrections	E53A	E53B
C_1 , Geometric detection efficiency	1.13 ± 0.01	1.13 ± 0.01
C_2 , Interaction before decay	1.16 ± 0.03	1.16 ± 0.03
C_3 , Low lifetime loss	1.13 ± 0.03	1.13 ± 0.03
C_4 , Slow decay prong	1.04 ± 0.01	1.04 ± 0.01
C_5 , Fake fits	0.95 ± 0.02	0.95 ± 0.02
C_6 , Random scan efficiency	0.98 ± 0.02	0.95 ± 0.02
C_7 , Reconstruction efficiency	0.98 ± 0.02	0.96 ± 0.02

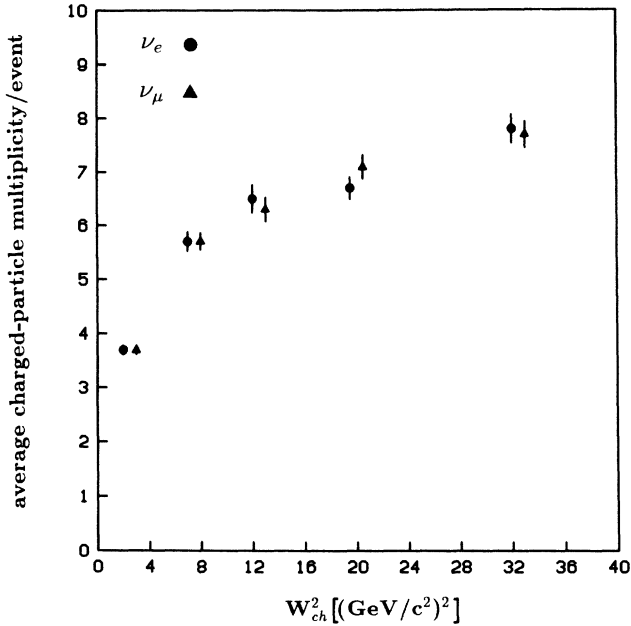


FIG. 7. The average charged-particle multiplicity for ν_e CC and ν_μ CC events plotted as a function of W_{ch}^2 .

momentum or neutral hadron energy measurement difficulties. For both the neutrinos and the antineutrinos, the agreement between the two neutrino types is very good, giving no evidence of a violation of universality.

E. Dileptons

A search was conducted for e^-e^+ (dilepton) events in the e^+ and e^- samples. These events are expected to

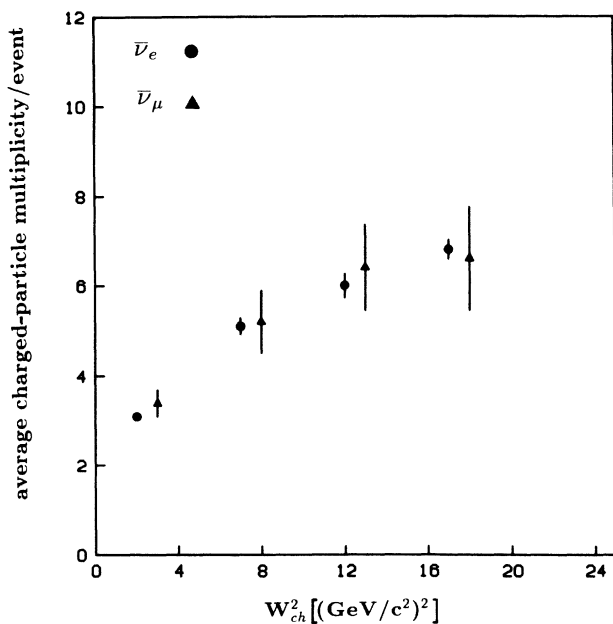


FIG. 8. The average charged-particle multiplicity for $\bar{\nu}_e$ and $\bar{\nu}_\mu$ CC events plotted as a function of W_{ch}^2 .

arise from ν_e -induced charm production and decay. A rate for this process has been reported only once previously.³⁰ The background to this process due to Dalitz pairs and close-in gamma conversions is severe. Requiring the candidate leptons to have high momenta and the e^-e^+ pair to have a large opening angle eliminated these backgrounds, leaving a signal consistent with universality.

The electron and positron samples were searched for events with at least one e^+ and one e^- track. These events were required to be inside the fiducial volume and to have no L^- track. The latter requirement eliminated the background from μ^-e^+ events. In addition, the e^- momentum was required to be greater than 5 GeV/c, the e^+ momentum was required to be greater than 1 GeV/c, the e^- had to pass the δ cut described in Sec. III, and the opening angle of the e^-e^+ pair was required to be greater than 8° . This search yielded a sample of five e^-e^+ events.

The possible backgrounds are wide-angle Dalitz pairs and close-in gamma conversions as well as ρ , ω , and ϕ meson decays. In order to pass the cuts imposed on the sample, the e^-e^+ pair must have at least 6 GeV in energy. In fact, the least energetic of the five pairs passing the cuts is 16 GeV. The multiplicity of π^0 's and gammas at these high energies is very low. Of the few high energy π^0 's only 1 in 80 Dalitz decay. The additional requirement that the opening angle be greater than 8° should eliminate this background.³¹ The possibility of poor angular resolution in the electron measurements allowing some events to pass the angle cut was investigated by examining 2500 zero opening angle pairs in charged-current ν_μ events. Only one of these pairs passed the cuts imposed on the e^-e^+ sample. Backgrounds due to decays of ρ and ω mesons were estimated from their respective mean multiplicities in neutrino interactions³² and branching ratios into states containing an e^- and an e^+ (Ref. 23). The e^-e^+ backgrounds from these decays were calculated to be 0.26 and 0.3 events, respectively. The background from decays of the ϕ meson were calculated in a similar manner. However, in this case a measured multiplicity in neutrino interactions was not available. The multiplicity was estimated by multiplying the ratio of the inclusive production of ϕ mesons to π^+ mesons in π^+p collisions by the average π^+ multiplicity in neutrino interactions.³³ The e^-e^+ background from ϕ decays was estimated to be 0.06 events. This gave a total estimated background in the e^-e^+ events of 0.6 ± 1.0 events.

Table V lists the momenta of the two leptons for each

TABLE V. Measured lepton momenta in e^-e^+ dilepton events.

Event	P_{e^-} (GeV/c)	P_{e^+} (GeV/c)
1	28.6	3.7
2	56.7	1.3
3	15.0	1.3
4	25.4	1.6
5	22.1	7.5

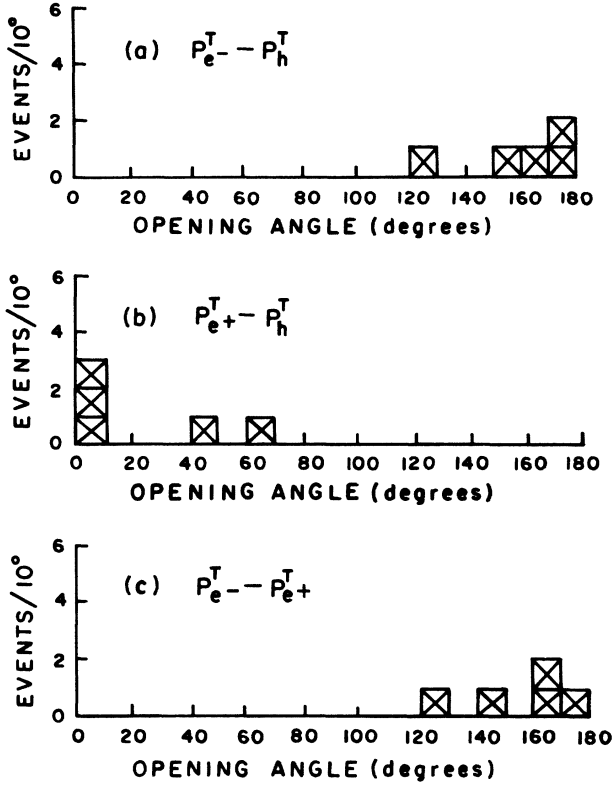


FIG. 9. Kinematic distributions for the e^-e^+ events. The angle between the transverse momenta of the e^- and the hadronic system is shown in (a). The angle between the transverse momenta of the e^+ and the hadronic system is shown in (b). (c) gives the angle between the transverse momenta of the e^- and the e^+ .

event in the e^-e^+ sample. The high e^- momenta and lower e^+ momenta are consistent with ν_e -induced charm production. In addition, there is kinematic evidence that the e^-e^+ events are from ν_e -induced charm. Figure 9(a) gives the angle between the transverse momenta (relative to the incident neutrino direction) of the hadronic system and the e^- . The hadronic system includes all tracks other than the two leptons. Figure 9(b) shows similar results for the hadronic system and the e^+ , and Fig. 9(c) gives that for the e^- and the e^+ . These plots indicate that the positron is produced in the hadronic sector of the event while the electron is produced apart from the hadronic sector. Similar plots can be seen in papers on μ^-e^+ and dimuon production.³⁴ This is consistent with the hypothesis that these events come from charm production by electron neutrinos.

The number of e^-e^+ events was corrected for losses and efficiencies. These corrections are summarized in Table VI. The corrections for the P_{e^+} cut and the opening angle cut were obtained by applying similar cuts to a sample of μ^-e^+ events. The other corrections are similar to those discussed in Sec. III. The corrected number (N_c) of e^-e^+ events is given by

$$N_c = N_o \frac{C_1 C_2 C_3 C_4 C_5 C_6}{C_7 C_8 C_9},$$

TABLE VI. Acceptance corrections and efficiencies for the e^-e^+ dilepton events.

	Correction
C_1 , delta ray	1.001 ± 0.001
C_2 , $P_{e^-} > 5$ GeV/c	1.17 ± 0.03
C_3 , $P_{e^+} > 1$ GeV/c	1.19 ± 0.03
C_4 , L^-	1.25 ± 0.05
C_5 , confused event	1.10 ± 0.05
C_6 , e^-e^+ opening angle $> 8^\circ$	1.5 ± 0.1
C_7 , scan efficiency	0.80 ± 0.05
C_8 , e^- identification efficiency	0.98 ± 0.02
C_9 , e^+ identification efficiency	0.96 ± 0.02

where N_o is the observed number of events and the C_i are as defined in Table VI. This yields a relative rate of

$$\frac{\nu_e N \rightarrow e^-e^+X}{\nu_e N \rightarrow e^-X} = \frac{(4.4 \pm 2.4)(3.9 \pm 0.7)}{2089 \pm 137} = (0.82 \pm 0.47)\%.$$

Although the corrections for confused events and scan efficiency cancel in the above ratio, they have been included so that the number of e^- events derived earlier in the paper can be used. The effect on the error is negligible. This e^-e^+ rate is comparable to the relative rate for μ^-e^+ production observed during this experiment³⁵

$$\frac{\nu_\mu N \rightarrow \mu^-e^+X}{\nu_\mu N \rightarrow \mu^-X} = (0.52 \pm 0.09)\% ,$$

as expected from universality. The observed e^-e^+ rate also agrees with the value of $(1.0_{-0.3}^{+1.9})\%$ observed by Balogh *et al.*³⁰

There were two observed V^0 's in the 5 e^-e^+ events. Correcting this number for V^0 losses and efficiencies as was done in Sec. IV C gives

$$\frac{\nu_e N \rightarrow e^-e^+V^0X}{\nu_e N \rightarrow e^-e^+X} = \frac{(2.0 \pm 1.4)(1.60 \pm 0.09)}{5.0} = 0.64 \pm 0.45 ,$$

consistent with the rate for muon neutrinos,³⁵

$$\frac{\nu_\mu N \rightarrow \mu^-e^+V^0X}{\nu_\mu N \rightarrow \mu^-e^+X} = 0.35 \pm 0.05 ,$$

as expected from universality. This high relative rate for strange-particle production is further evidence that the e^-e^+ events come from charm production.

V. CONCLUSIONS

In this paper a number of different tests of ν_μ - $\bar{\nu}_e$ and $\bar{\nu}_\mu$ - $\bar{\nu}_e$ universality are described. The ν_e and $\bar{\nu}_e$ samples used for these tests are an order of magnitude larger than those used in any previous high-energy experiment. The precision of these tests vary, ranging from 10% to 75%. No evidence for a violation of universality is seen. In addition, the rate for neutral-strange-particle production in e^-e^+ dilepton events is reported for the first time.

ACKNOWLEDGMENTS

We thank the scanning and measuring staffs at our institutions, as well as the operating crews of the 15-ft bub-

ble chamber and the neutrino beam at Fermilab. This research was supported by the U.S. Department of Energy and by the National Science Foundation.

- *Present address: Bear, Stearns, and Co., Inc., New York, NY 10167.
- †Present address: Yale University, New Haven, CT 06511.
- ‡Present address: Adelphi University, Garden City, NY 11530.
- §Present address: Seton Hall University, South Orange, NJ 07079.
- ¹Further details of this study can be found in S. Manly, Ph.D. thesis, Columbia University, 1988, Nevis Report No. 268.
- ²J. Calmet *et al.*, *Rev. Mod. Phys.* **49**, 21 (1977); J. Bailey *et al.*, *Phys. Lett.* **67B**, 225 (1977).
- ³D. E. Casperson *et al.*, *Phys. Rev. Lett.* **38**, 956 (1977); **38**, 1504 (1977); R. D. Ehrlich *et al.*, *Phys. Rev. A* **5**, 2357 (1972); S. J. Brodsky and G. W. Erickson, *Phys. Rev.* **148**, 26 (1966); F. Scheck, *Phys. Rep.* **44**, 187 (1978); J. L. Vuilleumier *et al.*, *Z. Phys. A* **278**, 109 (1976).
- ⁴A. Entenberg *et al.*, *Phys. Rev. Lett.* **32**, 486 (1974); I. Kostoulas *et al.*, *ibid.* **32**, 489 (1974); T. J. Braunstein *et al.*, *Phys. Rev. D* **6**, 106 (1972).
- ⁵D. P. Barber *et al.*, *Phys. Rev. Lett.* **43**, 1915 (1979).
- ⁶T. Kinoshita, *Phys. Rev. Lett.* **2**, 477 (1959); W. J. Marciano and A. Sirlin, *ibid.* **36**, 1425 (1976); D. A. Bryman *et al.*, *ibid.* **50**, 7 (1983).
- ⁷C. Albajar *et al.*, *Phys. Lett. B* **185**, 233 (1987). Also see recent results from the Collider Detector at Fermilab and Mark II Collaborations as well as results from the four experiments at the CERN e^+e^- collider LEP.
- ⁸D. Amidei *et al.*, *Phys. Rev. D* **37**, 1750 (1988); S. Abachi *et al.*, *Phys. Rev. Lett.* **59**, 2519 (1987); H. R. Band *et al.*, *ibid.* **59**, 415 (1987); Y. Tsai, *Phys. Rev. D* **4**, 2821 (1971).
- ⁹M. Klein, *Fortschr. Phys.* **33**, 375 (1985); B. Narkosa, in *Proceedings of the 1983 International Symposium on Lepton and Photon Interactions at High Energies*, Ithaca, New York, 1983, edited by D. G. Cassel and D. L. Kreinick (Newman Laboratory for Nuclear Studies, Cornell University, Ithaca, 1983).
- ¹⁰M. E. Duffy *et al.*, *Phys. Rev. Lett.* **52**, 1865 (1984); W. Droge *et al.*, *Nucl. Phys.* **B273**, 253 (1986); J. Dorenbosch *et al.*, *Phys. Lett. B* **180**, 303 (1986); J. Blietschau *et al.*, *Nucl. Phys.* **B133**, 205 (1978); O. Erriquez *et al.*, *Phys. Lett.* **102B**, 73 (1981); H. C. Ballagh *et al.*, *ibid.* **79B**, 320 (1978); V. V. Ammosov *et al.*, *Z. Phys. C* **40**, 487 (1988).
- ¹¹R. Barbieri, *Nucl. Phys.* **B269**, 253 (1986); R. Barbieri *et al.*, *Phys. Lett.* **156B**, 348 (1985).
- ¹²S. M. Bilenky and S. T. Petcov, *Rev. Mod. Phys.* **59**, 671 (1987).
- ¹³C. N. Leung, *Phys. Rev. D* **28**, 2205 (1983); M. Gronau, C. N. Leung, and J. L. Rosner, *ibid.* **29**, 2539 (1984); P. Ramond, *Nucl. Phys.* **B110**, 214 (1976); F. Gurse, P. Ramond, and P. Sikivie, *Phys. Lett.* **60B**, 177 (1976); T. G. Rizzo, *Phys. Rev. D* **34**, 1438 (1986); J. D. Bjorken and C. H. Llewellyn Smith, *ibid.* **7**, 887 (1973); C. W. Kim and J. Kim, *Phys. Lett.* **79B**, 278 (1978).
- ¹⁴S. Dimopoulos and J. Ellis, *Nucl. Phys.* **B182**, 505 (1981); R. N. Cahn and H. Harari, *ibid.* **B176**, 135 (1980).
- ¹⁵K. Enqvist, K. Mursula, and M. Roos, *Z. Phys. C* **21**, 133 (1983); J. Maalampi, K. Mursula, and M. Roos, *Nucl. Phys.* **B207**, 233 (1982).
- ¹⁶X. Li and E. Ma, *ibid.* **47**, 1788 (1981); E. Ma *et al.*, *ibid.* **60**, 495 (1988).
- ¹⁷TVGP and SQUAW were originally written by the Alvarez group at Berkeley. See F. T. Solmitz *et al.*, LRL Alvarez Group Programming Note No. P-117, 1966 (unpublished). For details on adaptation for use with the 15-ft bubble chamber, see E. E. Schmidt, Jr., Ph.D. thesis, Columbia University, 1978 Nevis Report No. 224.
- ¹⁸W. R. Nelson, H. Hirayama, and D. W. O. Rogers, SLAC Report No. 265, 1985 (unpublished).
- ¹⁹A. J. Malensek, Report No. FNAL-341, 2941.000, 1981 (unpublished).
- ²⁰H. W. Atherton *et al.*, CERN Report No. 80-07, 1980 (unpublished).
- ²¹T. Eichten *et al.*, *Nucl. Phys.* **B44**, 333 (1972).
- ²²J. Liu, Ph.D. thesis, Columbia University, 1985, Nevis Report No. 255.
- ²³Particle Data Group, *Rev. Mod. Phys.* **56**, S64 (1984).
- ²⁴B. Rossi, *High-Energy Particles* (Prentice-Hall, New York, 1952).
- ²⁵A. Buras and K. J. B. Gaemers, *Nucl. Phys.* **B132**, 249 (1978); A. Buras, *ibid.* **B125**, 125 (1977); A. De Rújula *et al.*, *ibid.* **B154**, 394 (1979). This code was obtained from C. Foudas of the CCFR Collaboration.
- ²⁶D. B. MacFarlane *et al.*, *Z. Phys. C* **26**, 1 (1984).
- ²⁷N. J. Baker *et al.*, *Phys. Rev. D* **34**, 1251 (1986).
- ²⁸V. V. Ammosov *et al.*, *Nucl. Phys.* **B177**, 365 (1981).
- ²⁹P. Bosetti *et al.*, *Nucl. Phys.* **B209**, 29 (1981).
- ³⁰H. C. Ballagh *et al.*, *Phys. Rev. D* **24**, 7 (1981).
- ³¹See B. Rossi, *High-Energy Particles* (Ref. 24); N. M. Kroll and W. Wada, *Phys. Rev.* **98**, 1355 (1955).
- ³²BEBC WA59 Collaboration, W. Wittek *et al.*, *Z. Phys. C* **44**, 175 (1989).
- ³³N. N. Biswas *et al.*, *Phys. Rev. D* **10**, 3579 (1974); P. Sixel *et al.*, *Nucl. Phys.* **B199**, 381 (1982).
- ³⁴N. J. Baker *et al.*, *Phys. Rev. D* **32**, 531 (1985); H. C. Ballagh *et al.*, *ibid.* **21**, 569 (1980); K. Lang *et al.*, *Z. Phys. C* **33**, 483 (1987); H. Abramowicz *et al.*, *ibid.* **15**, 19 (1982).
- ³⁵N. J. Baker *et al.*, *Phys. Rev. D* **32**, 531 (1985).